Adsorption of Hexavalent Chromium and Methylene Blue onto the Rubber Seed Shell Activated Carbon: Isotherm and Kinetic Studies

Kongsak Pattarith
Buriram Rajabhat University
Supattra Tangtubtim
Buriram Rajabhat University
Suphawarat Thupsuri (suphawarat.pl@bru.ac.th)
Buriram Rajabhat University https://orcid.org/0000-0001-8104-3755

Research Article

Keywords: Rubber seed shell, Charcoal , Activated carbon , Hexavalent chromium , Methylene blue

Posted Date: May 10th, 2022

DOI: https://doi.org/10.21203/rs.3.rs-1614108/v1

Adsorption of Hexavalent Chromium and Methylene Blue onto the Rubber Seed Shell Activated Carbon: Isotherm and Kinetic Studies

Kongsak Pattarith, Supattra Tangtubtim, Suphawarat Thupsuri*

ABSTRACT

Rubber seed shell (RSS) is a low-cost agricultural by-product. It has been utilized to produce two adsorbents, rubber seed shell charcoal (RSS-CH) and rubber seed shell activated carbon (RSS-AC) for removal of hexavalent chromium (Cr(VI)) and methylene blue (MB) from aqueous solutions. The surface morphology, thermal behavior, and FTIR were characterized to confirm the successful modification on the surface of the RSS. The effects of adsorption process such as pH, initial concentration, contact time, and temperature were also studied. The adsorption isotherm results revealed that the Langmuir isotherm model was a good fit for the Cr(VI) and MB adsorption processes. The Cr(VI) adsorption kinetic was explained by pseudo-first-order kinetic model and MB adsorption was followed with pseudo-second-order kinetic model. Moreover, the maximum adsorption capacities for Cr(VI) and MB adsorptions on the RSS-AC were 156.25 and 370.37 mg/g, respectively, which showed greater than those on the RSS-CH. Thus, the RSS-AC is a suitable, alternative, and high adsorption efficiency biosorbent for the removal of heavy metal and dye contaminants in wastewater.

Keywords:

Rubber seed shell

Charcoal

Activated carbon

Hexavalent chromium

Methylene blue

Article Highlights

- The adsorbents of RSS-CH and RSS-AC were utilized for removal of Cr(VI) and MB from aqueous solutions.
- The optimum conditions (pH, initial concentration, contact time, and temperature) were investigated to study the kinetic and isotherm adsorption processes for the Cr(VI) and MB adsorptions.
- The RSS-AC could be used as an alternative high-efficiency adsorbent for removal of Cr(VI) and MB.

ARTICLE INFO

Article history:

Received xx xxxx xxxx

Revised xx xxxx xxxx

Accepted xx xxxx xxxx

Available online xx xxxx xxxx

* Corresponding author

Contact: Suphawarat Thupsuri

E–mail address: *suphawarat.pl@bru.ac.th*

1 Introduction

At present, industrial waste from manufacturing processes, in either gas, liquid, or solid form depending upon the characteristics of the waste (Yin et al. 2019). It is released in excess into the environment. The discharge of wastewater containing heavy metals and dyes has become a particularly significant issue (Obiora-Okafo et al. 2022). Due to their complex molecular structures are low biodegradability and strong oxidation capability, pollutants cause severe damage to both human health and the ecosystem (Tran et al. 2015). They can transform into toxic or carcinogenic compounds (Abdeen and Mohammad 2014). Hexavalent chromium (Cr(VI)) originated from the wastewater of the electroplating, leather tanning, mining, textile, and ink industries (Liang et al. 2013; Hassanpour et al. 2018). It is one of the important heavy

metal pollutants present in the environment (Saha et al. 2011). Methylene blue (MB) is an organic dye with a positive electrical charge that is widely used for extensive application in the colorize substance especially in the textile industry (Manikandan et al. 2018; Pawar et al. 2018; Moradi 2014). The presence of Cr(VI) and MB in contaminated wastewater can adversely impact the health of human beings, fauna and flora, and aquatic ecosystems (Wang et al. 2020; Nguyen et al. 2013; Li et al. 2020; Kumar and Jena 2016; Liu et al. 2016). Therefore, the removal of such pollutants is necessary before the discharge of wastewater into natural bodies of water.

Adsorption has proved to be one of the most effective technics for the removal of toxic pollutant contaminated from industrial effluent (Cui et al. 2016; El-Enein et al. 2020; Wang et al. 2015). Several investigations on the development both of the natural and synthetic adsorbents for adsorption process have been performed (Choi 2019; Gómez et al. 2018; Hamami and Javanbakht 2021; Ghaedi et al. 2013). Activated carbon is extensively employed as an adsorbent due to its excellent properties such as high porosity large and surface area (El Nemr et al. 2021; Sultana et al. 2022; Mandal et al. 2021; Kumar et al. 2021; Saha et al. 2020). However, the raw materials commonly used to make activated carbon are expensive and difficult to regenerate. This has led to the use of agricultural waste in the production of activated carbon for heavy metal and dye removals from wastewater (Darweesh et al. 2022; Medhat et al. 2021; Thotagamuge et al. 2021). Rubber seed shell (RSS) is an agricultural waste material from natural rubber tree, which is widely cultivated in areas of Southeast Asia, including Thailand, Malaysia, and Philippines (Bhattacharjee et al. 2021). The latex rubber is a major product of the natural rubber tree, which is an extreme economic importance. Whereas, the potential usefulness of its by-product has previously attracted little attention. However, the huge amount of rubber seed shells generated during the cultivation of rubber trees has become an environmental problem for rubber tree plantations. This has led to RSS being chosen as a raw material for the preparation of low-cost adsorbent (Ekebafe et al. 2017; Sun and Jiang 2010).

The focus of this study is to investigate the adsorption potential of activated carbon from RSS using $ZnCl_2$ activation method. The RSS activated carbon (RSS-AC) was utilized for the removal of Cr(VI) and MB from aqueous solutions, and its adsorption performance compared to that of RSS charcoal (RSS-CH). The various parameters of pH, initial concentration, contact time, and temperature were evaluated. Isotherm and kinetic adsorptions were determined to

understand the adsorption process of Cr(VI) and MB onto the adsorbents. The regeneration efficiency of the adsorbents was also evaluated.

2 Materials and methods

2.1 Materials

Rubber seed shell (RSS) was the raw material used in this study. The collected seeds were first washed with distilled water and then dried at 110 ˚C overnight in an oven. The dried seeds were crushed to produce particles of the desired size of 2–4 mm. The crushed seeds were used as the precursor in the production of RSS-CH and RSS-AC. Zinc chloride, potassium dichromate, and methylene blue were purchased from Sigma Aldrich. All chemicals used are analytical grade.

2.2 Preparation of RSS-CH and RSS-AC

The RSS-AC was prepared through one-step chemical activation using $ZnCl_2$. The dried RSS precursor was mixed with 20% w/v $ZnCl_2$ at an impregnation ratio of 1:2 (w/v), sonicated for 1 h, and refluxed for a further 6 h. The sample was washed with distilled water until it became neutral pH and then dried at 110 °C overnight. The carbonization process was performed in an electric furnace at temperature of 600 °C for 3 h. Finally, the activated carbon was washed again with distilled water and then air dried at room temperature. The prepared RSS-AC was used for the adsorption studies of Cr(VI) and MB by comparison with adsorbent material of RSS-CH with non-activate carbon.

2.3 Characterization of materials

The samples of the RSS, RSS-CH, and RSS-AC were determined the surface functional groups by FTIR spectrometer (Spectrum GX-1, Perkin Elmer Co., Ltd., UK). The surface distribution parameters of the adsorbents were determined by BET technique (TriStar II Plus 3.00, Micromeritics Co., Ltd., USA) at 77 K using N_2 gas adsorption. Scanning electron

microscopy (TM40000Plus, Hitachi High-Tech Co., Ltd., Japan) was studied the surface morphology of the RSS, RSS-CH, and RSS-AC before adsorption. The thermal degradation characteristics of the adsorbents was evaluated by thermogravimetric (TG) analysis (SDT Q600, Lukens Drive, New Castle, DE 19720, USA) in N_2 atmosphere with a heating rate of 10 °C/min from ambient temperature up to 900 °C.

2.4 Adsorption experiments

The stock solutions of Cr(VI) and MB were prepared at concentration of 1000 mg/L. The pH values of these stock solution were adjusted by adding with 0.1 M HCl or 0.1 M NaOH. The stock solutions were stored for further adsorption studies. Batch adsorption experiments were conducted for investigation the Cr(VI) and MB adsorption behavior onto the RSS-CH and RSS-AC adsorbents. For each adsorption system, 50 mL of Cr(VI) or MB solutions was added with 0.01 g of adsorbent at various pH values under 150 rpm shaking and a controlled temperature of 30 °C for 3 h. The parameters of adsorption process of Cr(VI) and MB, *i.e.*, initial concentration, temperature, and contact time were investigated. The optimum conditions for the adsorptions of Cr(VI) and MB were used to determine the adsorption isotherm and kinetic studies. The concentration of the residual heavy metal and dye after the adsorption progress were analyzed by PerkinElmer Lambda 12 UV-Visible Spectrometer at wavelength of 540 and 664 nm for Cr(VI) and MB solutions, respectively. The adsorption capacity at equilibrium for Cr(VI) and MB adsorptions, q_e (mg/g), can be expressed by Eq. (1):

$$q_e = \frac{(C_i - C_e)}{M} V \tag{1}$$

where C_i and C_e are the concentration of heavy metal or dye solutions at initial and given contact time (mg/L), respectively. V is the volume of heavy metal or dye solutions (L) and M is the amount of adsorbent (g). The adsorption capacity at a time t, q_t (mg/g), was defined by Eq. (2):

$$q_t = \frac{(C_i - C_t)}{M} V \tag{2}$$

where C_t is the concentration at contact time t (mg/L). Each batch experiment was conducted in triplicate.

3 Results and discussion

3.1 Characterization

The functional group analysis of the RSS, RSS-CH, and RSS-AC samples is shown in Fig. 1. The FTIR spectra of RSS reveals that the broad peak at 3343 cm^{-1} is attributed to the O–H stretching vibration due to the presence of cellulose, lignin, and pectin. The peaks at 1705 and 1680 cm^{-1} are related with the C=O stretching vibration of carboxyl groups in hemicellulose (Zhuan et al. 2020). The sharp peak at 1027 cm^{-1} correspond to the C–O stretching for lignin characteristic. In contrast, the spectra of RSS-CH and RSS-AC are not only frequency-shifted but also feature additional peaks at 1560 cm^{-1} (C=C bonds), 1465 cm^{-1} (C–H bonds), and 1145 cm^{-1} (C–O bonds). These results indicate that the formation of new bands after the RSS carbonization and activation processes could be obviously changed in the functional groups of the RSS raw material (Lima et al. 2008).

The BET results of RSS-CH and RSS-AC were listed in Table 1. It is revealed that the surface area for RSS-AC is 267.13 m^2/g which shows greater than that of RSS-CH (255.23 m^2/g). The total pore volume of RSS-AC (0.15 cm^3/g) is also higher, suggesting that the surface structure of RSS was significantly damaged with $ZnCl_2$ agent during the activation procedure. The pores of RSS-CH and RSS-AC are 2.33 and 2.51 nm in diameter, respectively. The results imply that the material is predominantly mesoporous (Anyika et al. 2017). The surface morphologies of the RSS, RSS-CH, and RSS-AC are shown in Fig. 2. It can be seen that the RSS-CH and RSS-AC surfaces show numerous small pores, in comparison with the raw RSS material. Also, the surface of RSS under chemical activation procedure shows honeycomb-like porous structure due to the cellulose, hemicellulose, and lignin of RSS are destroyed via heat and $ZnCl_2$.

Fig. 3. shows the thermogravimetric (TG) and derivative (DTG) profiles for the RSS, RSS-CH, and RSS-AC samples. Owing to the evaporation of moisture, initial thermal degradation of all three samples appeared about 100 °C. The major weight loss of the RSS sample (270 – 600

°C) was decomposed on the main constituents of cellulose, hemicellulose, and lignin (Mandal et al. 2021). Moreover, TG curves for RSS-CH and RSS-AC exhibit more thermal stability than RSS, which may be the result of the dissociation of C–C bonds. These TG and DTG results also support that the surface of the RSS has been successfully modified.

3.2 Adsorption studies

3.2.1 Effect of pH

The effect of solution pH is an important parameter of bioadsorption process and it controls the electrostatic interaction between the modified adsorbent surface and the heavy metal as well as dye molecules. Heavy metal adsorption on the RSS-CH and RSS-AC was determined at pH values in the range of 2 to 7 with a concentration of 250 mg/L (Fig. 4a). Dye adsorption was studied at pH values in the range of 3 to 9 with concentration of 750 mg/L (Fig. 4b). For Cr(VI) adsorption, the acidic solution (pH = 3) was the optimum condition with adsorption capacity of 58.42 and 95.68 mg/g for Cr(VI) adsorption onto RSS-CH and RSS-AC, respectively. In a strongly acidic solution, a large number of anionic forms in the solution ($HCrO_4^-$ and $Cr_2O_7^{2-}$) have greater attraction toward the surface of adsorbent with positively charged adsorption sites, resulting in an increase of Cr(VI) adsorption capacity (Liu et al. 2017). With an increasing pH, the competition between the OH^- and anionic chromate ions occurs, leading to a decrease in adsorption capacity. Hence, the Cr(VI) adsorption efficiency is a suitable condition at low pH. For MB dye adsorption, the optimum condition in MB solution was pH 7 with adsorption capacity of 215.05 and 336.16 mg/g for MB adsorption onto RSS-CH and RSS-AC, respectively. Under acidic solution, the surface of the adsorbent is surrounded by H^+ ions leading to a weak interaction between the MB (cationic pollutant) and the adsorption sites, resulting in a decrease of the adsorption capacity for MB adsorbed on the surface. Thus, the MB adsorption efficiency is greatest at high pH values. This may be due to the electrostatic attraction between dye and adsorbent being strengthened with decreasing H^+ concentration (Ijagbemi et al. 2010).

3.2.2 Effect of initial concentration

To determine the effect of Cr(VI) and MB initial concentration onto the adsorbents, the initial Cr(VI) concentration was varied from 10 to 500 mg/L and the initial MB concentration from 10 to 1,000 mg/L. In Fig. 5, the adsorption capacity of Cr(VI) adsorbed on RSS-CH and RSS-AC rapidly increases and reaches an equilibrium at 250 mg/L. Similarly, the adsorption of MB reaches saturation at 750 mg/L. The enhanced adsorption efficiency with increasing initial concentration might be corresponded to the high utilization of available vacant site on the surface and adsorption rate of heavy metal and dye adsorptions. In addition, an increased initial concentration provides a powerful mass transfer between the adsorbate and adsorbent surface, resulting in higher adsorption capacity (Tuli et al. 2020).

3.2.3 Effect of contact time and temperature

The amount of Cr(VI) and MB adsorbed onto the adsorbent surfaces with different contact times at temperatures of 30, 40, and 50 °C is shown in Fig. 6. The Cr(VI) and MB adsorption capacity rapidly increase with the contact time of 60 min and 200 min, respectively. At higher contact times, the adsorption capacities gradually decrease in the later stages of adsorption because of the slow diffusion of heavy metal and dye particles through the solution to reach the internal pore adsorbent sites. When the temperature change from 30 to 50 °C, the amount of heavy metal and dye adsorptions decreased at high temperature because more kinetic energy of their molecules leading to an increase desorption efficiency on the surface (Ashokan et al. 2021).

3.3 Adsorption isotherms

The mechanisms of the adsorption at equilibrium are described with adsorption isotherm models. The Langmuir and Freundlich adsorption isotherms are extensively utilized to evaluate the interaction behavior during the adsorption process via the curve fitting method (Langmuir 1918). The Langmuir isotherm model assumes monolayer coverage of heavy metal and dye molecules onto the homogeneous surface. The linear form of the Langmuir equation is expressed by Eq (3):

$$\frac{C_e}{q_e} = \frac{C_e}{Q_m} + \frac{1}{bQ_m} \tag{3}$$

where C_e is the concentration equilibrium of heavy metal and dye (mg/L), q_e is the equilibrium adsorption capacity (mg/g), Q_m is the maximum adsorption capacity (mg/g), and b is the Langmuir binding constant (L/mg). A further analysis of the Langmuir hypothesis can be estimated using a dimensionless constant, (R_L), and it is expressed by Eq. (4):

$$R_L = \frac{1}{1 + bC_0} \tag{4}$$

where C_0 is the initial concentration of heavy metal and dye (mg/L). The R_L value describes the suitable for the adsorption isotherm in the present study, in which it is unfavorable ($R_L > 1$), favorable ($0 < R_L < 1$), linear ($R_L = 1$), and irreversible adsorption ($R_L = 0$). The value of 0 – 1 represents favorable for adsorption behavior (Table 2).

The Freundlich isotherm model is suitable for the heterogeneous adorption on the surface. The linear Freundlich equation is represented by Eq. (5) (Freundlich 1906):

$$\ln q_e = \ln K_F + \frac{1}{n} \ln C_e \tag{5}$$

where K_F and n are the Freundlich constant and Freundlich exponent, respectively, which n value relate to the adsorption capacity and adsorption strength.

The parameters of the Langmuir isotherm and Freundlich isotherm can be obtained from the corresponding slope and intercept of linearly plotting (Table 2). The adsorption isotherms of both Cr(VI) and MB on the surface provide a better fit for the Langmuir isotherm with a high correlation coefficient than for the Freundlich isotherm, indicating that the adsorption of heavy metal and dye onto the surfaces are distributed with monolayer coverage. Moreover, the Cr(VI) and MB adsorption efficiencies on the RSS-AC surface are higher than that of the RSS-CH surface, suggesting that the RSS-AC has a higher affinity binding sites.

3.4 Adsorption kinetics

To study the kinetic mechanisms in term of the order of the rate constant, pseudo-first-order and pseudo-second-order kinetics are applied (Ho and Mckay 1998). The linear form of the pseudo-first-order kinetic is calculated as follows:

$$\ln(q_e - q_t) = \ln q_e - k_1 t \quad (6)$$

where q_e and q_t are the amounts of heavy metal and dye adsorbed on the surface at equilibrium and at time t (mg/g), respectively. k_1 is pseudo-first-order adsorption constant (min^{-1}). In Table 3, the value kinetic parameters of k_1 and q_e can be obtained from the plot of $\ln(q_e - q_t)$ versus t with different temperatures (). The correlation coefficients of the pseudo-first-order model are greater than 0.99 for Cr(VI) adsorption onto the RSS-CH and RSS-AC when compare with the corresponding values for the pseudo-second-order model, indicating that the Cr(VI) adsorption obey the pseudo-second-order kinetic.

The linear form of the pseudo-second-order kinetic can be presented as follows:

$$\frac{t}{q_t} = \frac{1}{k_2 q_e^2} + \frac{t}{q_e} \quad (7)$$

where k_2 is the pseudo-second-order adsorption constant (g/mg.min). The kinetic parameters of k_2 and q_e can be obtained from the plot of $1/q_t$ versus t. The MB kinetic adsorption fit well with the pseudo-second-order model ($R^2 > 0.99$), implying that the adsorption rate is dependent on both adsorbate and adsorbent. It also shows that this adsorption process involves valence force via electron exchange between MB and surface.

3.5 Regeneration studies

The regenerative ability of an adsorbent in the desorption solution of 0.1 M HCl is an important for reducing the cost of the adsorption process. Fig. 7 shows that the reusability

potential of the surfaces was determined by repeating the adsorption of five cycles using 250 mg/L for the initial Cr(VI) concentration and 750 mg/L for the initial MB concentration at 30 °C for 3 h contact time. After 5 regenerations, the Cr(VI) and MB adsorption capacities on the RSS-CH decrease from 58.26 to 43.36 mg/g and 186.14 to 141.75 mg/g, respectively. While, the Cr(VI) and MB adsorption capacities on the RSS-AC decrease from 85.96 to 49.29 mg/g and 326.36 to 281.04 mg/g, respectively. The adsorption capacity of the adsorbents decreases with enhancing number of recycle times due to its the diminishing of active sites on the surface (Miraboutalebi et al 2017). Therefore, the effective bioadsorbent of RSS-CH and RSS-AC could be utilized as a recyclable adsorbent for the Cr(VI) and MB removal.

4 Conclusions

In this study, the prepared charcoal and activated carbon adsorbents by using a low-cost RSS as a raw material have been used for the Cr(VI) and MB removal from aqueous solutions. The modified adsorbent surfaces exhibited honeycomb-like porous structure due to its were destroyed via heat and activating agent. The equilibrium adsorption of Cr(VI) and MB on both RSS-CH and RSS-AC adsorbents showed a good fit in the Langmuir isotherm. The kinetic of Cr(VI) adsorption behavior was described by pseudo-first-order kinetic whereas the kinetic of MB adsorption explained by pseudo-second-order kinetic. The RSS-AC exhibited high adsorption efficiency when compared with RSS-CH. Therefore, the RSS-AC is the effective adsorbent for use in the removal of heavy metal and dye contaminants in wastewater.

Acknowledgement The authors gratefully acknowledge the Department of Chemistry, Faculty of Science Buriram Rajabhat University for the facilities provided.

Compliance with Ethical Standards

Author Contributions All authors designed and carried out the experiment. The experimental data was analyzed by Kongsak Pattarith. Suphawarat Thupsuri and Supattra Tangtubtim wrote the first draft of the manuscript. Finally, all authors approved the manuscript for the publication.

Funding The authors reported there is no funding associated for this study.

Data Availability All data are provided in this manuscript.

Declarations

Conflict of Interest There are no conflicts of financial interest.

References

Abdeen ZG, Mohammad S (2014) Study of the Adsorption Efficiency of an Eco-Friendly Carbohydrate Polymer for Contaminated Aqueous Solution by Organophosphorus Pesticide. Open J Org Polym Mater 4:16-28. https://doi.org/10.4236/ojopm.2014.41004

Anyika C, Asri NAM, Majid ZA, Yahya A, Jaafar J (2017) Synthesis and characterization of magnetic activated carbon developed from palm kernel shells. Nanotechnol Environ Eng 2:16. https://doi.org/10.1007/s41204-017-0027-6

Ashokan P, Asaithambi M, Sivakumar V, Sivakumar P (2021) Batch and column mode adsorption studies of reactive red 195 dye using Adenanthera paronina L seed activated carbon. Groundw Sustain Dev 15:100671. https://doi.org/10.1016/j.gsd.2021.100671

Bhattacharjee A, Bhowmik M, Paul C, Chowdhury BD, Debnath B (2021) Rubber tree seed utilization for green energy, revenue generation and sustainable development–A comprehensive review. Ind Crops Prod 174:114186. https://doi.org/10.1016/j.indcrop.2021.114186

Cui X, Hao H, Zhang C, He Z, Yang X (2016) Capacity and mechanisms of ammonium and cadmium sorption on different wetland-plant derived biochars. Sci Total Environ 539:566-575. https://doi.org/10.1016/j.scitotenv.2015.09.022

Choi HJ (2019) Applicability of Composite Beads, Spent Coffee Grounds/Chitosan, for the Adsorptive Removal of Pb(II) from Aqueous Solutions. Appl Chem Eng 30:536-545. https://doi.org/10.14478/ace.2019.1039

Darweesh MA, Elgendy MY, Ayad MI, Ahmed AMM, Elsayed NMK, Hammad WA (2022) Adsorption isotherm, kinetic, and optimization studies for copper (II) removal from aqueous solutions by banana leaves and derived activated carbon. S Afr J Chem Eng 40:10-20. https://doi.org/10.1016/j.sajce.2022.01.002

Ekebafe LO, Imanah JE, Okieimen FE (2017) Effect of carbonization on the processing characteristics of rubber seed shell. Arab J Chem 10:S174-S178. https://doi.org/10.1016/j.arabjc.2012.07.018

El-Enein SA, Okbah MA, Hussain SG, Soliman NF, Ghounam HH (2020). Adsorption of Selected Metals Ions in Solution Using Nano-Bentonite Particles: Isotherms and Kinetics. Environ Process 7:463–477. https://doi.org/10.1007/s40710-020-00430-x

El Nemr A, Shoaib AGM, El Sikaily A, Mohamed AEDA, Hassan AF (2021). Evaluation of Cationic Methylene Blue Dye Removal by High Surface Area Mesoporous Activated Carbon Derived from Ulva lactuca. Environ Process 8:311–332. https://doi.org/10.1007/s40710-020-00487-8

Freundlich H (1906) Uber die adsorption in Losungen. Zeitschrift für Physikalische Chemie. Z Phys Chem 57:385-470. https://doi.org/10.1515/zpch-1907-5723

Ghaedi M, Ghaedi AM, Abdi F, Roosta M, Vafaei A, Asghari A (2013) Principal component analysis- adaptive neuro-fuzzy inference system modeling and genetic algorithm optimization of adsorption of methylene blue by activated carbon derived from Pistacia khinjuk. Ecotoxicol. Environ Saf 96:110–117. https://doi.org/10.1016/j.ecoenv.2013.05.015

Gómez JM, Díez E, Bernabé I, Sáez P, Rodríguez A (2018). Effective Adsorptive Removal of Cobalt Using Mesoporous Carbons Synthesized by Silica Gel Replica Method. Environ Process 5:225–242. https://doi.org/10.1007/s40710-018-0304-9

Hamami Z, Javanbakht V (2021) Biosynthesis of copper oxide nanoparticles using biomass, peel, and extract polysaccharides of Solanum Tuberosum for ultrasound-assisted adsorption of azo direct red 80 contaminants. Ceram Int 47:24170-24181. https://doi.org/10.1016/j.ceramint.2021.05.128

Ho YS, Mckay G (1998) Sorption of dye from aqueous solution by peat. Chem Eng Sci 70:115-124. https://doi.org/10.1016/S0923-0467(98)00076-1

Hassanpour S, Taghizadeh M, Yamini Y (2018) Magnetic Cr(VI) Ion Imprinted Polymer for the Fast Selective Adsorption of Cr(VI) from Aqueous Solution. J Polym Environ 26:101-115. https://doi.org/10.1007/s10924-016-0929-6

Ijagbemi CO, Chun JI, Han D, Cho H, Se JO, Kim DS (2010) Methylene Blue adsorption from aqueous solution by activated carbon: Effect of acidic and alkaline solution treatments. J Environ Sci Health-Toxic/Hazard 45:958-967. https://doi.org/10.1080/10934521003772378

Kumar A, Jena HM (2016) Removal of methylene blue and phenol onto prepared activated carbon from Fox nutshell by chemical activation in batch and fixed-bed column. J Clean Prod 137:1246-1259. https://doi.org/10.1016/j.jclepro.2016.07.177

Kumar JA, Kumar PS, Krithiga T, Prabu D, Amarnath DJ, Sathish S, Venkatesan D, Hosseini-Bandegharaei A, Prashant P (2021) Acenaphthene adsorption onto ultrasonic assisted fatty

acid mediated porous activated carbon-characterization, isotherm and kinetic studies. Chemosphere 284:131249. https://doi.org/10.1016/j.chemosphere.2021.131249

Langmuir I (1918) The adsorption of gases on plane surfaces of glass, mica and platinum. J Am Chem Soc 40:1361-1403. https://doi.org/10.1021/ja02242a004

Li H, Liu L, Cui J, Cui J, Wang F, Zhang F (2020) High-efficiency adsorption and regeneration of methylene blue and aniline onto activated carbon from waste edible fungus residue and its possible mechanism. RSC Adv 10:14262-14273. https://doi.org/10.1039/d0ra01245a

Liang FB, Song YL, Huang CP, Zhang J, Chen BH (2013) Adsorption of hexavalent chromium on a lignin-based resin: Equilibrium, thermodynamics, and kinetics. J Environ Chem Eng 1:1301-1308. https://doi.org/10.1016/j.jece.2013.09.025

Lima EC, Royer B, Vaghetti JCP, Simon NM, da Cunha BM, Pavan FA, Benvenutti EV, Cataluña-Veses R, Airoldi C (2008) Application of Brazilian pine-fruit shell as a biosorbent to removal of reactive red 194 textile dye from aqueous solution. Kinetics and equilibrium study. J Hazard Mater 155:536-550. https://doi.org/10.1016/j.jhazmat.2007.11.101

Liu C, Jin RN, Ouyang XK, Wang YG (2017) Adsorption behavior of carboxylated cellulose nanocrystal-polyethyleneimine composite for removal of Cr(VI) ions. Appl Surf Sci 408:77-87. https://doi.org/10.1016/j.apsusc.2017.02.265

Liu F, Zou H, Hu J, Liu H, Peng J, Chen Y, Lu F, Huo Y (2016) Fast removal of methylene blue from aqueous solution using porous soy protein isolate based composite beads. Chem Eng Sci 287:410-418. https://doi.org/10.1016/j.cej.2015.11.041

Mandal S, Calderon J, Marpu SB, Omary MA, Shi SQ (2021) Mesoporous activated carbon as a green adsorbent for the removal of heavy metals and Congo red: Characterization, adsorption kinetics, and isotherm studies. J Contam Hydrol 243:103869. https://doi.org/10.1016/j.jconhyd.2021.103869

Manikandan G, Senthil Kumar P, Saravanan A (2018) Modelling and analysis on the removal of methylene blue dye from aqueous solution using physically/chemically modified Ceiba pentandra seeds. J Ind Eng Chem 62:446-461. https://doi.org/10.1016/j.jiec.2018.01.028

Medhat A, El-Maghrabi HH, Abdelghany A, Abdel Menem NM, Raynaud P, Moustafa YM, Elsayed MA, Nada AA (2021) Efficiently activated carbons from corn cob for methylene blue adsorption. Appl Surf Sci Adv 3:100037. https://doi.org/10.1016/j.apsadv.2020.100037

Miraboutalebi SM, Nikouzad SK, Peydayesh M, Allahgholi N, Vafajoo L, McKay G (2017) Methylene blue adsorption via maize silk powder: Kinetic, equilibrium, thermodynamic studies and residual error analysis. Process Saf Environ Prot 106:191–202. https://doi.org/10.1016/j.psep.2017.01.010

Moradi SE (2014) Microwave assisted preparation of sodium dodecyl sulphate (SDS) modified ordered nanoporous carbon and its adsorption for MB dye. J Ind Eng Chem 20:208-215. https://doi.org/10.1016/j.jiec.2013.04.005

Nguyen TAH, Ngo HH, Guo WS, Zhang J, Liang S, Yue QY, Li Q, Nguyen TV (2013) Applicability of agricultural waste and by-products for adsorptive removal of heavy metals from wastewater. Bioresour Technol 148:574-585. https://doi.org/10.1016/j.biortech.2013.08.124

Obiora-Okafo IA, Onukwuli OD, Igwegbe CA, Onu CE, Omotioma M (2022). Enhanced Performance of Natural Polymer Coagulants for Dye Removal from Wastewater: Coagulation Kinetics, and Mathematical Modelling Approach. Environ Process 9:20. https://doi.org/10.1007/s40710-022-00561-3

Pawar RP, Lalhmunsiama, Gupta P, Sawant SY, Shahmoradi B, Lee SM (2018) Porous synthetic hectorite clay-alginate composite beads for effective adsorption of methylene blue dye from aqueous solution. Int J Biol Macromol 114:1315-1324. https://doi.org/10.1016/j.ijbiomac.2018.04.008

Saha A, Basak BB, Ponnuchamy M (2020) Performance of activated carbon derived from Cymbopogon winterianus distillation waste for scavenging of aqueous toxic anionic dye Congo red: Comparison with commercial activated carbon. Sep Sci Technol 55:1970-1983. https://doi.org/10.1080/01496395.2019.1620277

Saha R, Nandi R, Saha B (2011) Sources and toxicity of hexavalent chromium. J Coord Chem 64:1782-1806. https://doi.org/10.1080/00958972.2011.583646

Sultana M, Rownok MH, Sabrin M, Rahaman MH, Alam SMN (2022) A review on experimental chemically modified activated carbon to enhance dye and heavy metals adsorption. Cleaner Eng Technol 6:100382. https://doi.org/10.1016/j.clet.2021.100382

Sun K, Jiang JC (2010) Preparation and characterization of activated carbon from rubber-seed shell by physical activation with steam. Biomass Bioenergy 34:539-544. https://doi.org/10.1016/j.biombioe.2009.12.020

Thotagamuge R, Kooh MRR, Mahadi AH, Lim CM, Abu M, Jan A, Hanipah AHA, Khiong YY, Shofry A (2021) Copper modified activated bamboo charcoal to enhance adsorption of heavy metals from industrial wastewater. Environ. Nanotechnol Monit Manag 16:100562. https://doi.org/10.1016/j.enmm.2021.100562

Tran VS, Ngo HH. Guo W. Zhang J, Liang S, Ton-That C, Zhang X (2015) Typical low cost biosorbents for adsorptive removal of specific organic pollutants from water. Bioresour Technol 182:353-363. https://doi.org/10.1016/j.biortech.2015.02.003

Tuli FJ, Hossain A, Kibria AKMF, Tareq ARM, Mamun SMMA, Ullah AKMA (2020) Removal of methylene blue from water by low-cost activated carbon prepared from tea waste: A study of adsorption isotherm and kinetics. Environ Nanotechnol Monit Manag 14:100354. https://doi.org/10.1016/j.enmm.2020.100354

Wang B, Lehmann J, Hanley K, Hestrin R, Enders A (2015) Adsorption and desorption of ammonium by maple wood biochar as a function of oxidation and pH. Chemosphere 138:120-126. https://doi.org/10.1016/j.chemosphere.2015.05.062

Wang Q, Zhou C, Kuang YJ, Jiang ZH, Yang M (2020) Removal of hexavalent chromium in aquatic solutions by pomelo peel. Water Sci Eng 13:65-73. https://doi.org/10.1016/j.wse.2019.12.011

Yin X, Jiang Y, Tan Y, Meng X, Sun H, Wang N (2019) Co-transport of graphene oxide and heavy metal ions in surface-modified porous media. Chemosphere 218: 1-13. https://doi.org/10.1016/j.chemosphere.2018.11.089

Zhuang J, Li M, Pu Y, Ragauskas AJ, Yoo CG (2020) Observation of potential contaminants in processed biomass using fourier transform infrared spectroscopy. Appl Sci 10:4345. https://doi.org/10.3390/app10124345

Affiliations

Kongsak Pattarith [1], Supattra Tangtubtim [1], Suphawarat Thupsuri [1]

Kongsak Pattarith
kongsak.pr@bru.ac.th

Supattra Tangtubtim
supattra.tt@bru.ac.th

Suphawarat Thupsuri
suphawarat.pl@bru.ac.th

[1] *Department of Chemistry, Buriram Rajabhat University, Buriram, Thailand*

Figure captions

Fig. 1 FTIR spectrum for (**a**) RSS, (b) RSS-CH, and (**c**) RSS-AC.

Fig. 2 SEM images of (**a**) RSS, (**b**) RSS-CH, and (**c**) RSS-AC.

Fig. 3 (**a**) Dynamic TG and (**b**) DTG curves of RSS, RSS-CH, and RSS-AC under a heating rate of 10 °C/min in nitrogen.

Fig. 4 Effect of pH value for (**a**) Cr(VI) and (**b**) MB adsorptions on RSS-CH and RSS-AC.

Fig. 5 Effect of initial concentration for (**a**) Cr(VI) and (**b**) MB adsorptions on RSS-CH and RSS-AC.

Fig. 6 Effect of contact time and temperature for Cr(VI) adsorption on (**a**) RSS-CH and (**b**) RSS-AC. Effect of contact time and temperature for MB adsorption on (**c**) RSS-CH and (**d**) RSS-AC.

Fig. 7 Regeneration plot of (**a**) Cr(VI) and (**b**) MB adsorptions.

Table 1

Surface distribution parameters of RSS-CH and RSS-AC.

Adsorbent	BET surface area (m^2/g)	Total pore size (cm^3/g)	Average pore diameter (nm)
RSS-CH	255.23	0.14	2.51
RSS-AC	267.13	0.15	2.33

Table 2

Langmuir and Freundlich isotherm parameters for the Cr(VI) and MB adsorptions on the RSS-CH and RSS-AC.

Adsorbent	Langmuir equation				Freundlich equation		
	R_L	Q_m (mg/g)	b (ml/mg)	R^2	K_F (L/g)	n (L/mg)	R^2
Cr(VI) adsorption							
RSS-CH	0.75	126.58	0.0013	0.9952	7.10	1.0458	0.9772
RSS-AC	0.67	156.25	0.0020	0.9950	3.71	1.0106	0.9902
MB adsorption							
RSS-CH	0.17	222.22	0.0064	0.9860	1.62	0.9247	0.9733
RSS-AC	0.14	370.37	0.0085	0.9920	1.31	1.0289	0.9912

Table 3

Pseudo-first-order and Pseudo-second-order kinetic parameters for the Cr(VI) and MB adsorptions on the RSS-CH and RSS-AC.

Adsorbent	T(°C)	q_e (exp.) (mg/g)	Pseudo-first-order			Pseudo-second-order		
			q_e (cal.) (mg/g)	k_1 (min^{-1})	R^2	q_e (cal.) (mg/g)	K_2 (g/mg.min)	R^2
Cr(VI) adsorption								
RSS-CH	30	58.79	60.04	0.0635	0.9965	90.09	0.0004	0.9060
	40	47.14	49.18	0.0572	0.9915	96.15	0.0002	0.9126
	50	33.89	36.35	0.0507	0.9830	23.75	0.0002	0.8600
RSS-AC	30	88.70	69.71	0.0518	0.9994	74.62	0.0003	0.9837
	40	75.02	65.60	0.0623	0.9998	72.46	0.0002	0.9758
	50	50.47	51.16	0.0647	0.9984	75.19	0.0008	0.9901
MB adsorption								
RSS-CH	30	186.94	12.24	0.0086	0.7730	40.32	0.0053	0.9993
	40	174.10	11.62	0.0085	0.7459	36.36	0.0054	0.9996
	50	161.80	11.58	0.0086	0.6803	34.24	0.0073	0.9992
RSS-AC	30	326.73	224.07	0.0455	0.8656	200.00	0.0042	0.9994
	40	306.05	232.29	0.0427	0.7935	172.41	0.0035	0.9983
	50	256.45	195.19	0.0439	0.7673	174.05	0.0039	0.9962

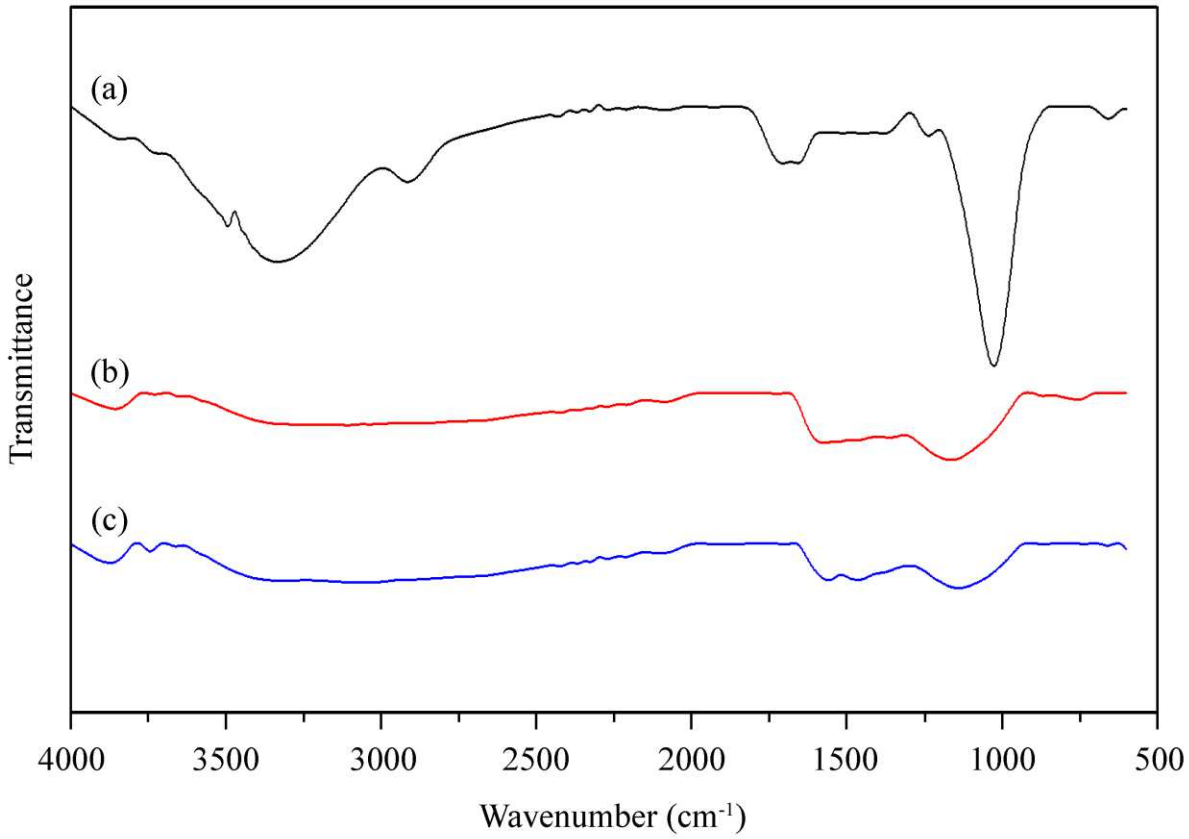

Fig. 1 FTIR spectrum for (**a**) RSS, (**b**) RSS-CH, and (**c**) RSS-AC.

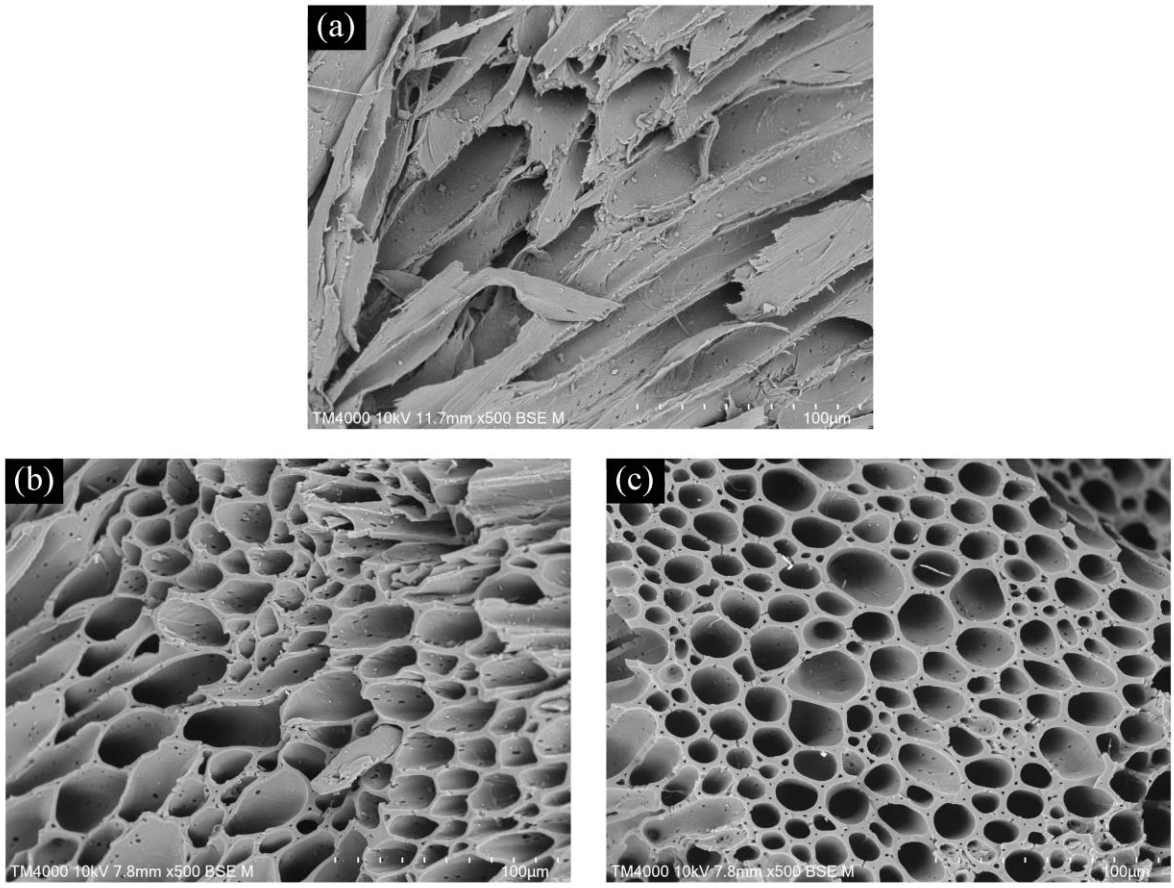

Fig. 2 SEM images of (**a**) RSS, (**b**) RSS-CH, and (**c**) RSS-AC.

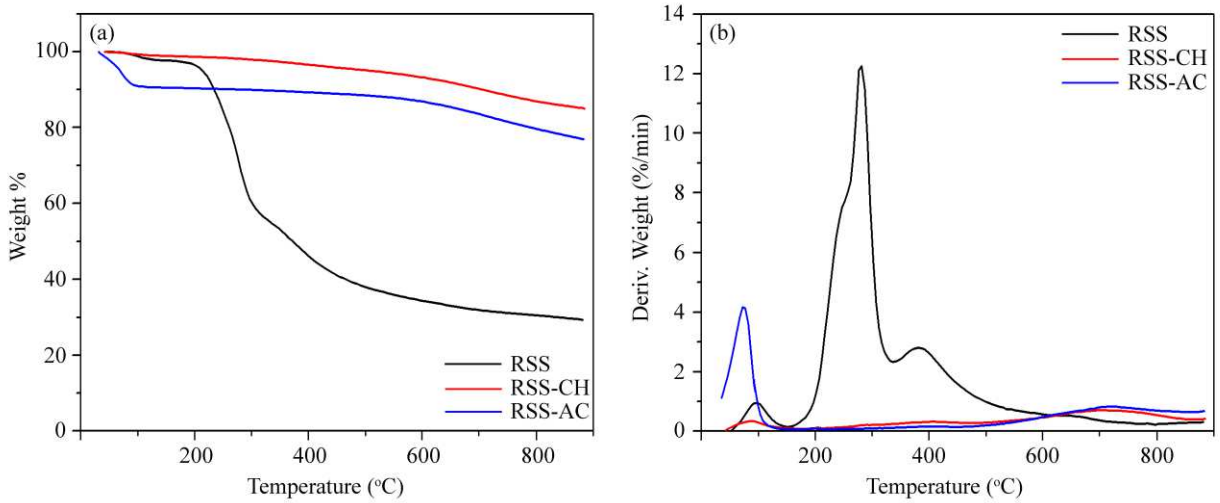

Fig. 3 (**a**) Dynamic TG and (**b**) DTG curves of RSS, RSS-CH, and RSS-AC under a heating rate of 10 °C/min in nitrogen.

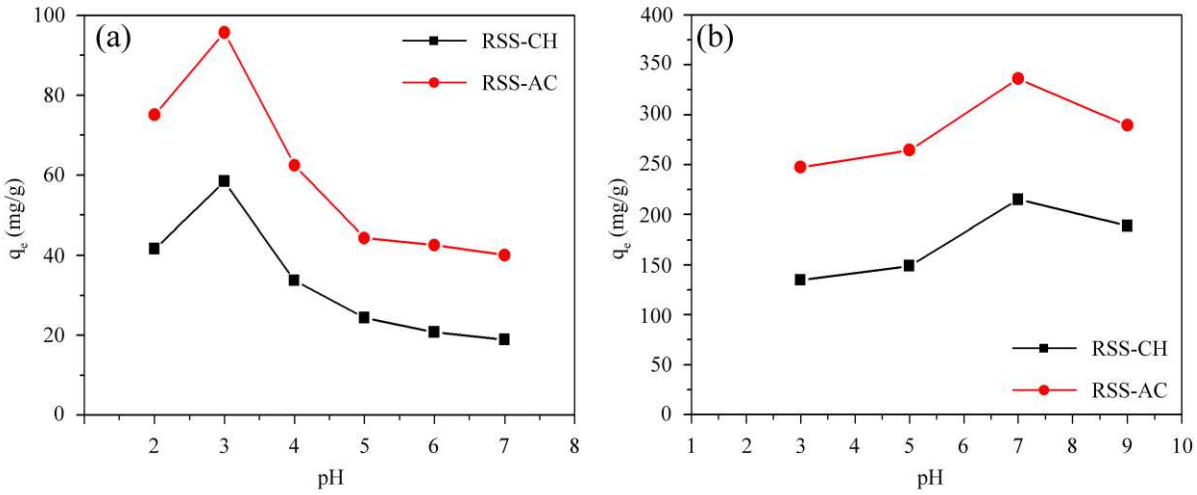

Fig. 4 Effect of pH value for (**a**) Cr(VI) and (**b**) MB adsorptions on the RSS-CH and RSS-AC.

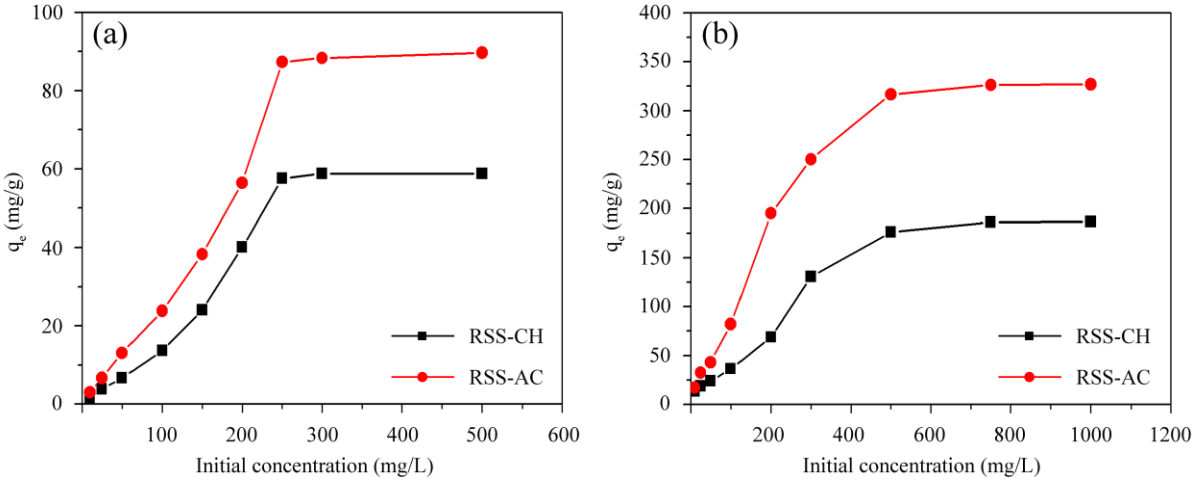

Fig. 5 Effect of initial concentration for (**a**) Cr(VI) and (**b**) MB adsorptions on the RSS-CH and RSS-AC.

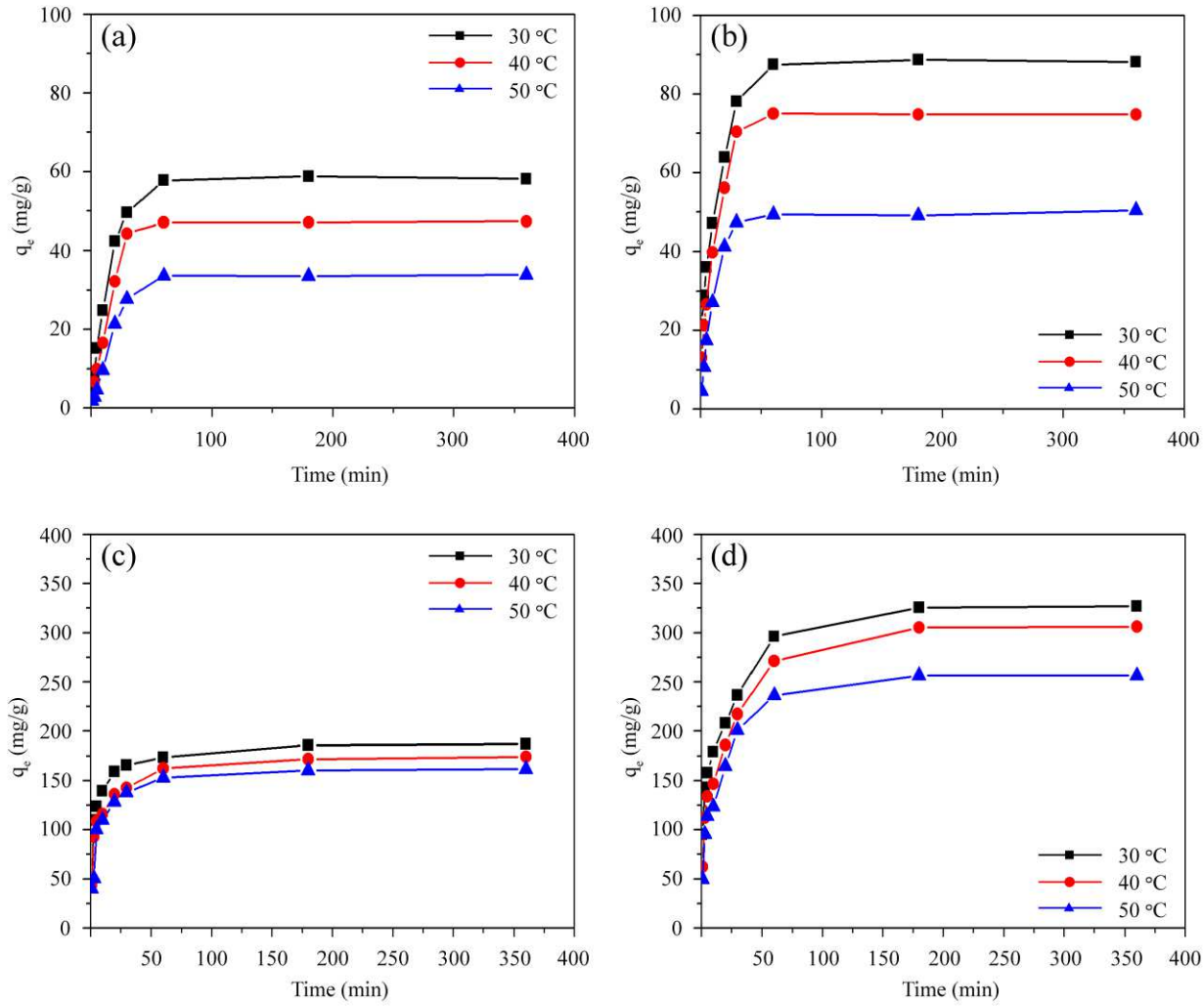

Fig. 6 Effect of contact time and temperature for Cr(VI) adsorption on the (**a**) RSS-CH and (**b**) RSS-AC. Effect of contact time and temperature for MB adsorption on the (**c**) RSS-CH and (**d**) RSS-AC.

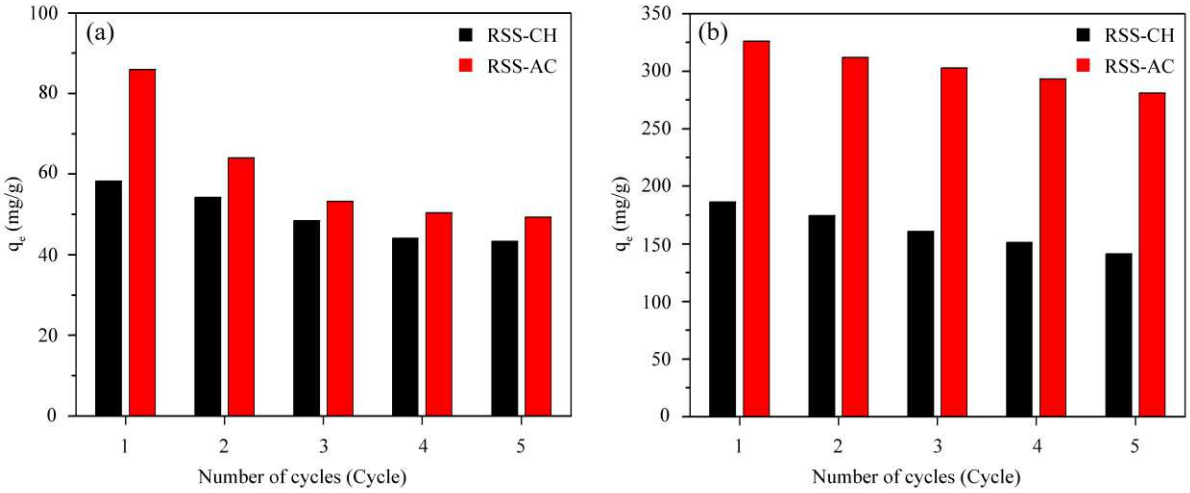

Fig. 7 Regeneration plot of (**a**) Cr(VI) and (**b**) MB adsorptions.